

# Large-scale non-Gaussian mass function and halo bias: tests on N-body simulations

M. Grossi<sup>1</sup>, L. Verde<sup>2,3</sup>, C. Carbone<sup>3</sup>, K. Dolag<sup>1</sup>, E. Branchini<sup>4</sup>, F. Iannuzzi<sup>1,5</sup>, S. Matarrese<sup>6</sup>, L. Moscardini<sup>5,7</sup>

<sup>1</sup>*Max-Planck Institut fuer Astrophysik, Karl-Schwarzschild Strasse 1, D-85748 Garching, Germany (margot,dolag,iannuzzi@mpa-garching.mpg.de)*

<sup>2</sup>*ICREA*

<sup>3</sup>*Institute of Space Sciences (CSIC-IEEC), UAB, Barcelona 08193, Spain (verde,carbone@ieec.uab.es)*

<sup>4</sup>*Dipartimento di Fisica, Università di Roma TRE, via della Vasca Navale 84, I-00146, Roma, Italy (branchin@fis.uniroma3.it)*

<sup>5</sup>*Dipartimento di Astronomia, Università di Bologna, via Ranzani 1, I-40127 Bologna, Italy (lauro.moscardini@unibo.it)*

<sup>6</sup>*Dipartimento di Fisica "G. Galilei", Università degli Studi di Padova and INFN Sezione di Padova, via Marzolo 8, I-35131, Padova, Italy (sabino.matarrese@pd.infn.it)*

<sup>7</sup>*INFN, Sezione di Bologna, viale Berti Pichat 6/2, I-40127 Bologna, Italy*

30 May 2018

## ABSTRACT

The description of the abundance and clustering of halos for non-Gaussian initial conditions has recently received renewed interest, motivated by the forthcoming large galaxy and cluster surveys, which can potentially yield constraints of order unity on the non-Gaussianity parameter  $f_{NL}$ . We present tests on N-body simulations of analytical formulae describing the halo abundance and clustering for non-Gaussian initial conditions. We calibrate the analytic non-Gaussian mass function of Matarrese et al. (2000) and LoVerde et al. (2008) and the analytic description of clustering of halos for non-Gaussian initial conditions on N-body simulations. We find excellent agreement between the simulations and the analytic predictions if we make the corrections  $\delta_c \rightarrow \delta_c \times \sqrt{q}$  and  $\delta_c \rightarrow \delta_c \times q$  where  $q \simeq 0.75$ , in the density threshold for gravitational collapse and in the non-Gaussian fractional correction to the halo bias, respectively. We discuss the implications of this correction on present and forecasted primordial non-Gaussianity constraints. We confirm that the non-Gaussian halo bias offers a robust and highly competitive test of primordial non-Gaussianity.

**Key words:** methods: statistical, N-body simulations–cosmology: theory, large-scale structure of universe galaxies: clusters: general – galaxies: halos

## 1 INTRODUCTION

Constraining primordial non-Gaussianity offers a powerful test of the generation mechanism of cosmological perturbations in the early universe. While standard single-field models of slow-roll inflation lead to small departures from Gaussianity, non-standard scenarios allow for a larger level of non-Gaussianity (Bartolo et al. (2004) and references therein). The standard observables to constrain non-Gaussianity are the Cosmic Microwave Background (CMB) and the Large Scale Structure (LSS) of the Universe. A powerful technique is based on the abundance (Matarrese et al. 2000; Verde et al. 2001; LoVerde et al. 2008; Koyama et al. 1999; Robinson & Baker 2000; Robinson et al. 2000) and clustering (Grinstein & Wise 1986; Matarrese et al. 1986; Lucchin et al. 1988) of rare events, such as dark matter density peaks, as they trace the tail of the underlying

matter distribution. Theoretical predictions on various observational aspects of non-Gaussianity have been extensively tested against N-body simulations, leading to different and sometimes conflicting results (Kang et al. 2007; Grossi et al. 2007; Dalal et al. 2007; Desjacques et al. 2008; Pillepich et al. 2008).

Dalal et al. (2007) and Matarrese & Verde (2008) showed that primordial non-Gaussianity affects the clustering of dark matter halos inducing a scale-dependent bias on large scales. Not only this effect has been already exploited to place stringent constraints on non-Gaussianity (Slosar et al. 2008; Afshordi & Tolley 2008), but also it is particularly promising for constraining non-Gaussianity from future surveys, which will provide a large sample of galaxy clusters over a volume comparable to the horizon size (e.g., DES, PanSTARRS, BOSS, LSST, ADEPT, EUCLID) (Dalal et al. 2007; Carbone et al. 2008; Afshordi & Tolley

2008; Seljak 2008). Bartolo et al. (2005) showed that even for small primordial non-Gaussianities, the evolution of perturbations on super-Hubble scales yields extra contributions. The amplitude of these contributions is comparable to the forecasted errors of some planned surveys, opening up the possibility of measuring them.

In light of this, it is important to use N-body experiments to test the validity of theoretical predictions for halo-bias in non-Gaussian framework. Indeed, all proposed analytic biasing expressions have been derived in the extended Press-Schechter framework which assumes spherical collapse dynamics, sharp k-space filtering and Gaussian initial conditions. The validity of the extrapolation of the extended Press-Schechter approach to the non-Gaussian case can be tested independently by considering also the halo mass function. It is thus also important to test and calibrate on N-body simulations the predictions of the non-Gaussian halo mass function (Kang et al. 2007; Grossi et al. 2007; Dalal et al. 2007) and of the non-Gaussian halo bias simultaneously. This is what we set out to do here.

In this paper we start by reviewing the analytic predictions for the Gaussian and non-Gaussian halo abundance and clustering (§2). In §3 we describe the numerical simulations with Gaussian and non-Gaussian initial conditions. In §4 we present the test for the non-Gaussian mass function. In §5 and 6 we test the analytic predictions of Gaussian and non-Gaussian large scale bias against N-body simulations. In §7 we compare our results with the literature. Finally, we conclude in §8.

## 2 FORMULATION OF THE NON-GAUSSIAN HALO ABUNDANCE AND CLUSTERING

Deviations from Gaussian initial conditions are commonly parameterized in terms of the dimensionless  $f_{\text{NL}}$  parameter (Salopek & Bond 1990; Gangui et al. 1994; Verde et al. 2000; Komatsu & Spergel 2001):

$$\Phi = \phi + f_{\text{NL}}(\phi^2 - \langle \phi^2 \rangle), \quad (1)$$

where  $\Phi$  denotes the gravitational potential and  $\phi$  is a Gaussian random field. As noted by e.g., LoVerde et al. (2008), Afshordi & Tolley (2008) and Pillepich et al. (2008), different authors use different conventions. Here  $\Phi$  denotes Bardeen's gauge-invariant potential which, on sub-Hubble scales, reduces to the usual Newtonian peculiar gravitational potential but with a negative sign. In addition, there are two conventions for normalizing Eq. (1): the LSS and the CMB one. In the LSS convention  $\Phi$  is linearly extrapolated at  $z = 0$ . In the present paper we use this convention. In the CMB convention  $\Phi$  is instead primordial: thus  $f_{\text{NL}} = [g(z = \infty)/g(0)]f_{\text{NL}}^{\text{CMB}} \sim 1.3f_{\text{NL}}^{\text{CMB}}$ , where  $g(z)$  denotes the linear growth suppression factor in non Einstein-de-Sitter Universes.

### 2.1 Formulation of the non-Gaussian mass function: Extended Press-Schechter approach

In the Press-Schechter framework, one considers the density contrast field evaluated at some early time, far before any scale of interest has approached the nonlinear regime, but extrapolated to the present day using linear perturbation

theory. Then one considers the height of the critical density threshold as a function of time. In that way, the collapse of a halo at redshift  $z \neq 0$  corresponds to the  $z = 0$  density fluctuation crossing a barrier of height  $\delta_c(z) = \Delta_c D(z = 0)/D(z)$ , where  $\Delta_c \sim \delta_c(z = 0)$  (this is an equality only in an Einstein de Sitter Universe); we use  $D(z = 0) = 1$ ,  $D(z) = g(z)/g(0)(1+z)^{-1}$ . We should recall here that, even in linear theory, the normalized skewness of the density field,  $S_3 \equiv \langle \delta^3 \rangle / \langle \delta^2 \rangle^2$ , depends on redshift  $\propto 1/D(z)$ , however in the Press-Schechter framework one should use the linear  $S_3(z = 0)$ , in what follows  $S_3 \equiv S_3(z = 0)$ . Note also that in general the skewness can be written as  $S_3 \equiv f_{\text{NL}} S_3^{(1)}$ , where  $S_3^{(1)}$  denotes the skewness in units of  $f_{\text{NL}}$ , care must be exercised in the interpretation of  $f_{\text{NL}}$ : if  $S_3^{(1)}$  is that of the density field linearly extrapolated at  $z = 0$ ,  $f_{\text{NL}}$  must be the LSS one and *not* the CMB one.

Generalization of the mass function to non-Gaussian initial conditions within the Press-Schechter formalism has been presented in Matarrese et al. (2000); LoVerde et al. (2008). Both references start by computing an expression for the non-Gaussian probability density function of the smoothed dark matter density field, then obtain the level excursion probability. In the Press-Schechter approach the mass derivative of the level excursion probability is the key ingredient to obtain the mass function expression and is the term that gets modified in the presence of primordial non-Gaussianity. In this derivation, several approximations are made. Both approaches assume that deviations from Gaussianity are small.

Matarrese et al. (2000) use first the saddle-point approximation to compute the level excursion probability and then truncate the resulting expression at the skewness. They obtain <sup>1</sup>:

$$n(M, z) = 2 \frac{3H_0^2 \Omega_{m,0}}{8\pi G M^2} \frac{1}{\sqrt{2\pi}\sigma_M} \exp\left[-\frac{\delta_*^2}{2\sigma_M^2}\right] \times \quad (2)$$

$$\left| \frac{1}{2} \frac{\delta_c^2}{3\sqrt{1 - S_{3,M}\delta_c/3}} \frac{dS_{3,M}}{d \ln M} + \frac{\delta_*}{\sigma_M} \frac{d\sigma_M}{d \ln M} \right|$$

where  $\sigma_M$  denotes the *rms* value of the density field, the subscript  $M$  denotes that the density field has been smoothed on a scale  $R(M)$  corresponding to  $R(M) = [M3/(4\bar{\rho}_M)]^{1/3}$ , and  $\delta_* = \delta_c \sqrt{1 - \delta_c S_{3,M}/3}$ .

LoVerde et al. (2008) instead first approximate the probability density function using the Edgeworth expansion, then perform the integral of the level excursion probability exactly on the first few terms of the expansion. They obtain:

$$n(M, z) = 2 \frac{3H_0^2 \Omega_{m,0}}{8\pi G M^2} \frac{1}{\sqrt{2\pi}\sigma_M} \exp\left[-\frac{\delta_c^2}{2\sigma_M^2}\right] \times \quad (3)$$

$$\left[ \frac{d \ln \sigma_M}{dM} \left( \frac{\delta_c}{\sigma_M} + \frac{S_{3,M}\sigma_M}{6} \left( \frac{\delta_c^4}{\sigma_M^4} - 2 \frac{\delta_c^2}{\sigma_M^2} - 1 \right) \right) \right. \\ \left. + \frac{1}{6} \frac{dS_{3,M}}{dM} \sigma_M \left( \frac{\delta_c^2}{\sigma_M^2} - 1 \right) \right]$$

Note that in the limit of small non-Gaussianity and rare events, the ratio of the non-Gaussian mass function to the Gaussian one for both expressions reduces to:

<sup>1</sup> We correct here a typo in Eq. (68) of Matarrese et al. (2000), where  $d \ln \sigma_M$  should be  $d\sigma_M$ .

$$\mathcal{R}_{NG} \equiv \frac{n(M, z|f_{NL})}{n(M, z|f_{NL}=0)} \longrightarrow 1 + S_{3,M} \frac{\delta_c^3}{6\sigma_M^2}. \quad (4)$$

It is important to bear in mind that in Eqs. (3)-(4), the redshift dependence is enclosed only in  $\delta_c$  (and not in  $S_3$ ). In the spirit of the ‘‘CMB’’ convention instead, where the gravitational potential is normalized deep in the matter era, one should make sure that all the relevant quantities are correctly extrapolated linearly at  $z = 0$ , keeping in mind that the gravitational potential slowly evolves in a non Einstein de Sitter Universe.

The major limitations in both derivations are the assumption of spherical collapse and the sharp  $k$ -space filtering. In addition, the excursion set improvement on the interpretation of the original Press-Schechter swindle, suggests that this derivation relies on the random-phase hypothesis Sheth (1998), which is clearly not satisfied for non-Gaussian initial conditions even for sharp  $k$ -space filtering.

Verde et al. (2001) and LoVerde et al. (2008) addressed this issue by using the analytical approach to compute the fractional non-Gaussian correction to the Gaussian mass function  $\mathcal{R}_{NG}$ , and used the Sheth & Tormen (1999) mass function to model the Gaussian mass function. This approach is potentially promising, but needs to be calibrated on numerical experiments.

In particular, one may argue that the same correction that in the Gaussian case modifies the collapse threshold and thus the form of the mass function from Press & Schechter (1974) to Sheth et al. (2001) and Sheth & Tormen (2002), may apply to the non-Gaussian correction. In the Gaussian case this is usually referred to as the correction due to ellipsoidal collapse (Lee & Shandarin 1998). While this interpretation has recently been disputed (see e.g., Robertson et al. (2008)), we will maintain the same nomenclature here. For rare events, high peaks ( $\delta_c/\sigma_M \gg 1$ ) and small  $f_{NL}$ , this is equivalent to lower  $\delta_c$  by a factor  $\sqrt{q}$  with  $q = 0.75$ .

In summary we propose that the non-Gaussian mass function  $n(M, z, f_{NL})$  should be re-written in terms of the Gaussian one  $n_G^{sim}(M, z)$  –given by tested fits to simulations e.g., Sheth & Tormen (1999); Reed et al. (2003); Warren et al. (2006); Jenkins et al. (2001)–, multiplied by a non-Gaussian correction factor:

$$n(M, z, f_{NL}) = n_G^{sim}(M, z) \times \mathcal{R}_{NG}(M, z, f_{NL}) \quad (5)$$

where  $\mathcal{R}_{NG}(M, z, f_{NL})$  takes two different forms in the Matarrese et al. (2000) and LoVerde et al. (2008) approximations. For the Matarrese et al. (2000) case <sup>2</sup>

$$\mathcal{R}_{NG}(M, z, f_{NL}) = \exp \left[ \delta_{ec}^3 \frac{S_{3,M}}{6\sigma_M^2} \right] \times \left[ \frac{1}{6} \frac{\delta_{ec}^2}{\sqrt{1 - \delta_{ec} S_{3,M}/3}} \frac{dS_{3,M}}{d \ln \sigma_M} + \frac{\delta_{ec} \sqrt{1 - \delta_{ec} S_{3,M}/3}}{\delta_{ec}} \right] \quad (6)$$

and for the LoVerde et al. (2008) case:

$$\mathcal{R}_{NG}(M, z, f_{NL}) = 1 + \frac{1}{6} \frac{\sigma_M^2}{\delta_{ec}} \times \left[ S_{3,M} \left( \frac{\delta_{ec}^4}{\sigma_M^4} - 2 \frac{\delta_{ec}^2}{\sigma_M^2} - 1 \right) + \frac{dS_{3,M}}{d \ln \sigma_M} \left( \frac{\delta_{ec}^2}{\sigma_M^2} - 1 \right) \right] \quad (7)$$

<sup>2</sup> We correct here a typo in Eq. (3) of Grossi et al. (2007) where the exponential part was missing.

where  $\delta_{ec}$  denotes the critical density for ellipsoidal collapse, which for high peaks is  $\delta_{ec} \sim \delta_c \sqrt{q}$  with  $q = 0.75$ .

## 2.2 Formulation of the non-Gaussian large scale halo bias

For the case of ‘‘local’’ primordial non-Gaussianity Eq. (1), the analytical expression for the large-scale non-Gaussian bias has been derived in five different ways, obtaining always basically the same result. Dalal et al. (2007) considered the Laplacian of  $\Phi$  in the vicinity of rare, high peaks, considering that the resulting  $\nabla^2 \Phi$  is proportional to the peaks overdensity; they also generalized to local non-Gaussianity the Kaiser (1984) argument of high-peaks bias in order to derive its non-Gaussian version. Matarrese & Verde (2008) derived the halo bias formula in general non-Gaussian cases specified by an expression for the bispectrum. Slosar et al. (2008) adopted the peak-background split approach (Cole & Kaiser 1989) for the local non-Gaussian case, showing that the resulting expression relies on the universality of the mass function. Afshordi & Tolley (2008) instead interpreted non-Gaussianity as a modification of the critical density for collapse, in the framework of ellipsoidal collapse. Finally, McDonald (2008) used a renormalized perturbation theory approach to consider at the same time non-linear bias, second-order gravitational evolution and local form of non-Gaussianity. It is encouraging that these different approaches yield a consistent result for the correction to the Gaussian Lagrangian halo bias  $b_L^G$ :

$$\frac{\Delta b}{b_L^G} = 2f_{NL} \delta_c(z) \alpha_M(k) \quad (8)$$

where  $\alpha_M(k)$  encloses the scale and halo mass dependence –see e.g., Eq. (13) and Fig. 3 of Matarrese & Verde (2008)–. Also in this case the density field is the one extrapolated linearly at  $z = 0$ , and  $\alpha_M$  does not depend on redshift.

Making the standard assumption that halos move coherently with the underlying dark matter, the Lagrangian bias is related to the Eulerian one as  $b = 1 + b_L$ .

The approximations used to derive this equation are Press-Schechter (Press & Schechter 1974) approach, linear bias, small non-Gaussianity, and in most cases spherical collapse and identification of peaks with halos. It is therefore important to test the validity of Eq. (8), with simulations and see if any correction factor needed is indeed due to account for non-spherical collapse. Following the derivation of Matarrese & Verde (2008) we recognize that the correction to the 2-point halo correlation function due to non-Gaussianity (their Eq. (6)) is multiplied by  $\nu^3/\sigma_M^3$  with  $\nu = \delta_c/\sigma_M$ . In this factor we recognize one Lagrangian Gaussian bias factor to the second power and an extra  $\delta_c/\sigma_M^2$ , which denominator was absorbed in the form factor. Recall that, as discussed in §2.1, for ‘‘ellipsoidal collapse’’ and rare events, the Lagrangian Gaussian bias is corrected as  $\nu/\sigma_M \longrightarrow q\nu/\sigma_M$  (see Eq. (11) below, for high  $\nu$ ). However, the remaining factor is also a Gaussian bias and it should also be corrected by the  $q$ -factor.

We conclude that the ‘‘non-spherical collapse’’ modifies Eq. (8) to be:

$$\frac{\Delta b}{b_L^G} \simeq 2f_{NL} \delta_c(z) \alpha_M(k) q. \quad (9)$$

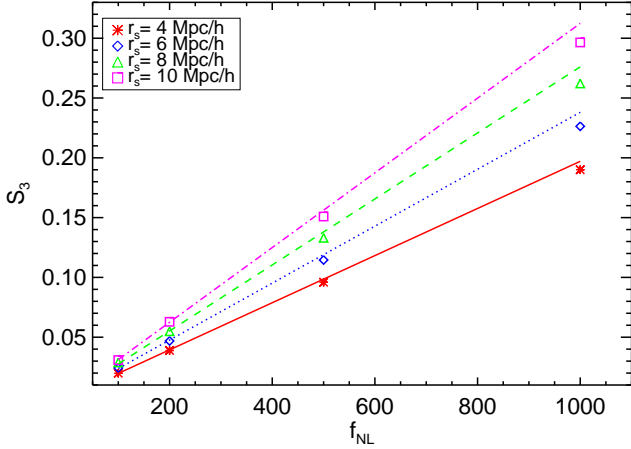


**Figure 1.** Skewness  $S_3$  of the smoothed initial density field for  $f_{\text{NL}} = 100, 200, 500, 1000$ . Symbols show the numerical results of the initial conditions code (averaged over 5 realizations) and are plotted against the analytical predictions for smoothing radii  $r_s = 4, 6, 8, 10 \text{ Mpc}/h$  of a spherical top-hat filter.

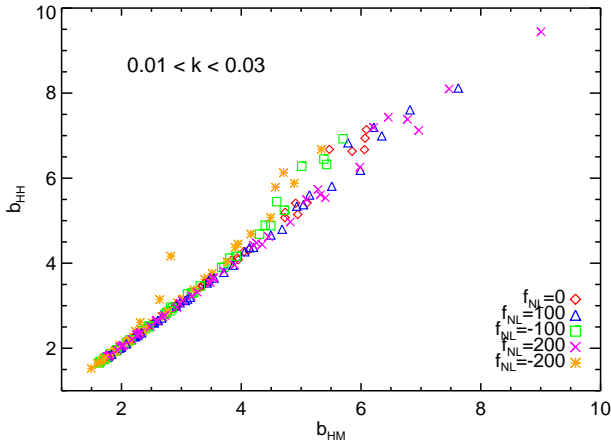


**Figure 2.** The bias of the halo power spectrum  $b_{hh}$  compared to the bias of the cross (halo-matter) power spectrum  $b_{hm}$ . As expected, when the number density of halos is high there is good agreement between the two quantities. At low halo number densities the two quantities are affected differently by shot noise, with  $b_{hm}$  being the least affected.

Note that Afshordi & Tolley (2008) arrived to a similar yet not identical expression when considering ellipsoidal collapse, i.e. they suggest that  $\delta_c$  should be substituted by the critical density of Sheth et al. (2001), which in our limit would correspond to use  $\sqrt{q}$  rather than  $q$  in Eq. (9).

In §6 we will show that Eq. (9) correction fits well the simulations.

### 3 N-BODY SIMULATIONS

The deviations from Gaussianity we are after become important on very large scales  $k \lesssim 0.03h/\text{Mpc}$  and for massive halos. Therefore, one needs to perform N-body simulations

on very large boxes, yet with enough resolution to identify massive virialized structures at different redshifts.

Suitable initial conditions have been set up following the method described in more detail in Grossi et al. (2008) (see also Grossi et al. (2007); Viel et al. (2009)). In brief, a random realization of a Gaussian gravitational potential,  $\Phi_L$ , normalized to be the one linearly extrapolated at  $z = 0$ , is generated in Fourier space, then it is inverse-Fourier transformed back to real space and added to the non-Gaussian term,  $\Phi_{\text{NL}} = f_{\text{NL}} (\Phi_L^2 - \langle \Phi_L^2 \rangle)$ . The resulting field  $\Phi_L + \Phi_{\text{NL}}$  that is linear and at  $z = 0$ , is transformed back in Fourier space. We eventually modulate the power-law spectrum using the transfer function and compute the corresponding density field, which we then scale back to the initial conditions redshift ( $z = 60$ ). The corresponding gravitational potential is then used to displace particles according to the Zel'dovich approximation. This method allows one to simulate non-Gaussian models having power spectra which are all consistent with that of the Gaussian case and was already used by Viel et al. (2009).

In order to check the reliability of the initial conditions generation, we have performed a specific test: using  $256^3$  particles in a box of size  $1000 \text{ Mpc}/h$ , primordial density fields (extrapolated linearly at  $z = 0$ ) were generated and smoothed using spherical top-hat filters of different radii  $r_s = 4, 6, 8, 12 \text{ Mpc}/h$ . The smoothed skewness was then extracted from the fields and compared to the analytical prediction for  $f_{\text{NL}} = 100, 200, 500, 1000$ , as shown in Figure 1.

The set of simulations used in this work assumes the ‘concordance’  $\Lambda\text{CDM}$  model. We fix the relevant parameters consistently with those derived from the analysis of the WMAP 5-year data (Komatsu et al. 2008):  $\Omega_{m0} = 0.26$  for the matter density parameter,  $\Omega_{\Lambda0} = 0.74$  for the  $\Lambda$  contribution to the density parameter,  $h = 0.72$  for the Hubble parameter (in units of  $100 \text{ km s}^{-1} \text{ Mpc}^{-1}$ ). The initial power spectrum adopts the Cold Dark Matter (CDM) transfer function suggested by Eisenstein & Hu (1999), has a spectral index  $n = 0.96$  and is normalized in such a way that  $\sigma_8 = 0.8$ . In all experiments, performed using the GADGET-2 numerical code (Springel 2005), switching off the hydrodynamical part, we consider a box of  $(1200 \text{ Mpc}/h)^3$  with  $960^3$  particles: the corresponding particle mass is then  $m \approx 1.4 \times 10^{11} h^{-1} M_{\odot}$ . The gravitational force has a Plummer-equivalent softening length of  $\epsilon_l = 25h^{-1} \text{ kpc}$ . The runs produced 15 outputs from the initial redshift ( $z = 60$ ) to the present time. The 5 simulations consider different amounts of primordial non-Gaussianity, parametrized by the  $f_{\text{NL}}$  parameter:  $f_{\text{NL}} = 0$  (i.e. the reference Gaussian case) and  $f_{\text{NL}} = \pm 100, \pm 200$ . The catalogues of dark matter haloes are extracted from the simulations using the standard friends-of-friends algorithm adopting a linking length of 0.2 times the mean interparticle distance; only objects with at least 32 particles are considered.

We thus measure the halo bias in the simulations as

$$b_s(k, M, z) = b_{hm} \equiv \frac{P_{hm}(k, z, M)}{P_{mm}(k, z)}, \quad (10)$$

where  $P_{hm}(k, z, M)$  denotes the cross-power spectrum of dark matter with halos of mass  $M$  at scale  $k$ , and for the simulation snapshot at redshift  $z$ . Similarly  $P_{mm}(k, z)$  denotes the dark matter power spectrum. Here and hereafter

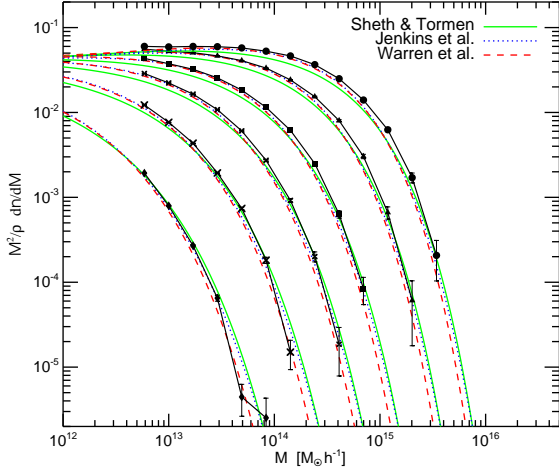


**Figure 3.** Multiplicity mass function for the Gaussian simulation computed using a Friends-of-Friends halo finder. Points denote the simulations results at different redshift:  $z = 0, 0.44, 1.02, 1.53, 2.26$  and  $3.23$  (top to bottom). Solid (green) lines are the Sheth & Tormen (1999) formula, dashed (red) lines are the Warren et al. (2006) one and dotted (blue) are the Jenkins et al. (2001).

the subscript  $s$  denotes quantities measured from the simulation.

In principle, the quantity one is interested in would be the bias of the halo power spectrum  $b_{hh} = \sqrt{P_{hh}/P_{mm}}$ , but  $b_{hm}$  is a less noisy quantity (the shot noise of the finite number of halos is greatly suppressed in the estimate of  $P_{hm}(k)$ ). The quantity  $b_{hm}$  is not guaranteed to be identical to  $b_{hh}$  if bias has a stochastic component that does not correlate with the matter density field. In Fig. 2 we show that this is not the case and that there is good agreement on large scales between  $b_{hh}$  and  $b_{hm}$ , justifying using the less noisy  $b_{hm}$  as an estimator for  $b_{hh}$ .

### 3.1 Comparison with independent simulations

In Fig. 3 we show the mass function extracted from our Gaussian simulations at the following redshifts:  $z = 0.0, 0.44, 1.02, 1.53, 2.26$  and  $3.23$ . We also show three different theoretical predictions (also calibrated on  $N$ -body simulations): Sheth & Tormen (1999); Jenkins et al. (2001); Warren et al. (2006), solid, dotted and dashed lines respectively. There is good agreement even at high redshift.

Several groups recently presented  $N$ -body simulations, aiming at quantifying the effect of the non Gaussian initial conditions on the halo mass function (Desjacques et al. 2008; Pillepich et al. 2008). All these results are obtained for similar cosmological parameters, so that we can compare estimates derived from all the simulations directly. By comparing the results for the individual simulations at  $z = 1$ ,  $z \sim 0.5$  and  $z = 0$  in Figures 4, 5 we demonstrate that these results are in agreement among the different groups, once the  $f_{NL}$  values are suitably converted to the same convention. Although all simulations use boxes of Giga parsec scales to explore the effect of non-Gaussian initial conditions at the high mass end, the statistical errors at the scale of massive clusters are still large. Therefore, we also report the recip-

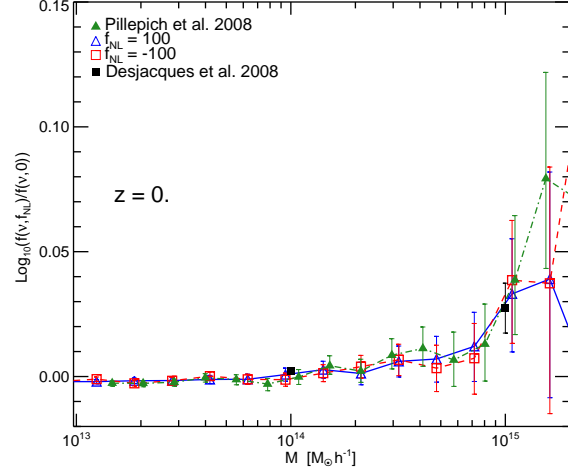


**Figure 4.** Comparison between the halo mass function recovered in our simulations with the work of Desjacques et al. (2008) and Pillepich et al. (2008) at  $z = 0$ . We show the ratio between our non-Gaussian and Gaussian simulation with  $f_{NL} = \pm 100$ , few points we read out from Figure 1 of Desjacques et al. (2008) (black points) at the values of  $\nu$  corresponding to  $1 \times 10^{13}, 1 \times 10^{14}$  and  $1 \times 10^{15} M_{\odot}/h$  and the points from Pillepich et al. (2008). We plot the reciprocal of the results for  $f_{NL} = -100$ .

rocal of the results obtained for negative  $f_{NL}$  so that they appear in the positive part of the plot, to give an intuitive feeling of the noise within the individual simulations.

In Figure 4, we show our simulation results for  $f_{NL} = 100$  (blue triangles) and for  $f_{NL} = -100$  (red squares) at  $z = 0$  compared with data points from Figure 1 of Desjacques et al. (2008) (black points) at the values of  $\nu$  corresponding to  $1 \times 10^{13}, 1 \times 10^{14}$  and  $1 \times 10^{15} M_{\odot}/h$  (as given in their figure caption). Note that, as Desjacques et al. (2008) use  $f_{NL} = 100$  in the CMB convention for their simulations, we scaled the points down accordingly by a factor 1.3 to be comparable with our  $f_{NL} = 100$ . We also show the results for Pillepich et al. (2008) (green points). Here we again apply the re-scaling as before, as their  $f_{NL}$  of 82 would correspond to a  $f_{NL}$  of  $\sim 106$  in the LSS notation.

In Figure 5, the left panel shows the results for Pillepich et al. (2008) (green points) at  $z = 0.5$ , and our points for the two closest available output times of our simulation ( $z = 0.44$  and  $z = 0.61$ ). The right panel shows the comparison at  $z = 1$  between our points (blue triangles and red squares) and points from Desjacques et al. (2008) (black squares).

From this comparison we conclude that there is remarkable agreement between the three independent simulations, highlighting the robustness of the simulations results. The differences visible at some of the highest mass bins are not significant, given the large error bars present.

## 4 MASS FUNCTION

We compare the halo mass function of the non-Gaussian simulations with the theoretical predictions of Eqs. (5), (6) and (7) that is, including our *ansatz* for the non-spherical collapse correction:  $\delta_c \rightarrow \sqrt{q}\delta_c$ . For clarity we show here

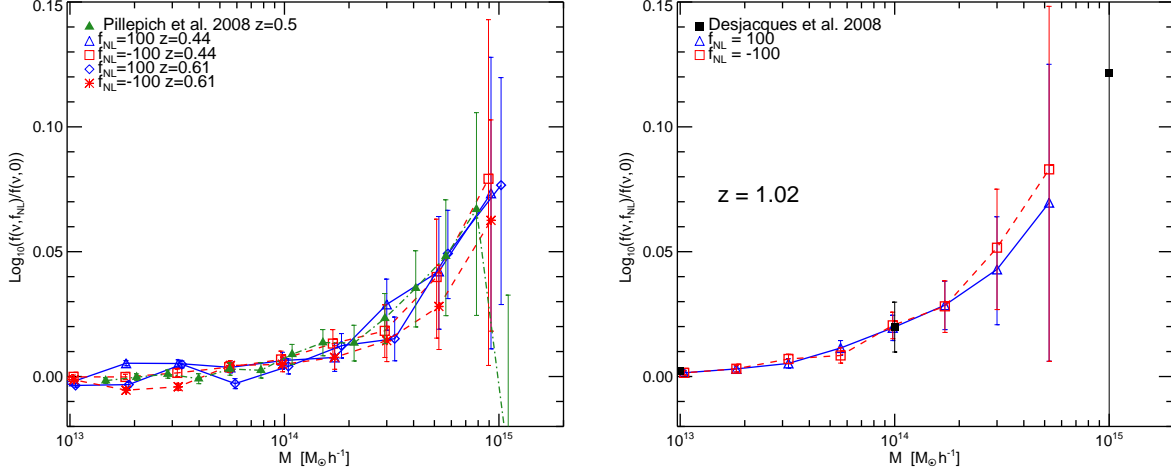


**Figure 5.** Comparison between the halo mass function recovered in our simulations with the work of Desjacques et al. (2008) and Pillepich et al. (2008). In the left panel we show the ratio between the non-Gaussian and Gaussian simulation at redshift 1 for our simulations with  $f_{NL} = \pm 100$ , three points we read out from Figure 1 of Desjacques et al. (2008) (black points) at the values of  $\nu$  corresponding to  $1 \times 10^{13}$ ,  $1 \times 10^{14}$  and  $1 \times 10^{15} M_{\odot}/h$ . We plot the reciprocal of the results for  $f_{NL} = -100$ . In the right panel we show the data of Pillepich, Porciani, Hahn (2008) at  $z = 0.5$  and we compare them with our simulation results for the two closest available redshifts :  $z = 0.44$  and  $z = 0.61$  and with Desjacques et al. (2008). All points are rescaled to  $|f_{NL} = 100|$  in our notation. The three independent simulations are in good agreement.

the non-Gaussian to Gaussian mass function ratio, i.e. the factor  $R_{NG}(M, z)$ . The comparison between theory and simulations results is shown in Fig. 6 for a few redshift snapshots and for  $f_{NL} = \pm 100$ , and in Fig. 7 for  $f_{NL} = \pm 200$  for the same redshifts. Dashed lines are the mass function of Matarrese et al. (2000)–Eq. (6) – and dot-dashed lines are that of LoVerde et al. (2008)–Eq. (7)–.

Contrary to Kang et al. (2007) and Dalal et al. (2007), we conclude that both Matarrese et al. (2000) and LoVerde et al. (2008) are good descriptions of the non-Gaussian correction to the mass function, once the correction for non-spherical collapse is included.

Figs. 6 and 7 seem to indicate that LoVerde et al. (2008) may be a better fit for small masses and Matarrese et al. (2000) at high masses. This is not surprising: the Edgeworth expansion works well away from the extreme tails of the distribution (i.e. for moderate  $\delta_c/\sigma_M$ ), while the saddle-point-approximation used in Matarrese et al. (2000), is expected to work better at the very tails of the distribution (very high  $\delta_c/\sigma_M$ ). We expect that the mass function of Matarrese et al. (2000) will be a better fit at very high masses or larger  $f_{NL}$ . This will be further explored in future work.

## 5 GAUSSIAN HALO BIAS, AND THE EFFECT OF MERGERS

The large-scale, linear halo Eulerian bias for the Gaussian case is (Mo et al. 1997; Scoccimarro et al. 2001)

$$b^G = 1 + \frac{1}{D(z_o)} \left[ \frac{q\delta_c(z_f)}{\sigma_M^2} - \frac{1}{\delta_c(z_f)} \right] + \quad (11)$$

$$\frac{2p}{\delta_c(z_f)D(z_o)} \left[ 1 + \left( \frac{q\delta_c^2(z_f)}{\sigma_M^2} \right)^p \right]^{-1},$$

where  $q = 0.75$  and  $p = 0.3$ , account for non-spherical collapse and are a fit to numerical simulations. Here,  $\sigma_M$  denotes the *rms* value of the dark matter fluctuation field smoothed on a scale  $R$  corresponding to the Lagrangian radius of the halos of mass  $M$ ;  $z_f$  denotes the halo formation redshift and  $z_o$  denotes the halo observation redshift. As we are interested in massive halos, we expect that  $z_f \simeq z_o$ . As the non-Gaussian halo bias correction is proportional to  $b^G - 1$ , the dependence of  $b^G$  on whether the selected halos underwent a recent merger (i.e.  $z_f \sim z_o$ ) or are old halos (i.e.  $z_f \gg z_o$ ) affects the amplitude of the non-Gaussian correction (Slosar et al. 2008; Carbone et al. 2008). Before we trust our simulation to accurately describe the non-Gaussian halo bias we check whether we recover the Gaussian one and whether the linear halo bias approximation is a good description for the scales, redshifts and mass-ranges we are interested in. Gao et al. (2005) show that analytical predictions for the Gaussian halo bias are in reasonable agreement with simulations and that the bias for low-mass halos shows strong dependence on formation time but high mass halos (the ones we are interested in) do not. The halo bias for the Gaussian simulation and the comparison with the theory prediction is shown in Fig. 8. Except for the Gaussian halo bias  $b_0^G \equiv 1 + \delta_c(z_o)/(\sigma_M^2 D(z_o))$  defined in Efstathiou et al. (1988) and Kaiser (1984) indicated by the dotted (blue) line, the simulated data agree with the theoretical expectations at different redshifts. In particular, in Fig. 8, the black solid line represents the total Gaussian bias of Eq. (11), the dashed (red) line represents the contribution from the first line of Eq. (11), and, finally, the dot-dashed (green) line is  $1 + q(b_0^G - 1)$ . The small difference when using  $z_f \sim z_o$  implies that, for the Gaussian halo bias of very massive halos

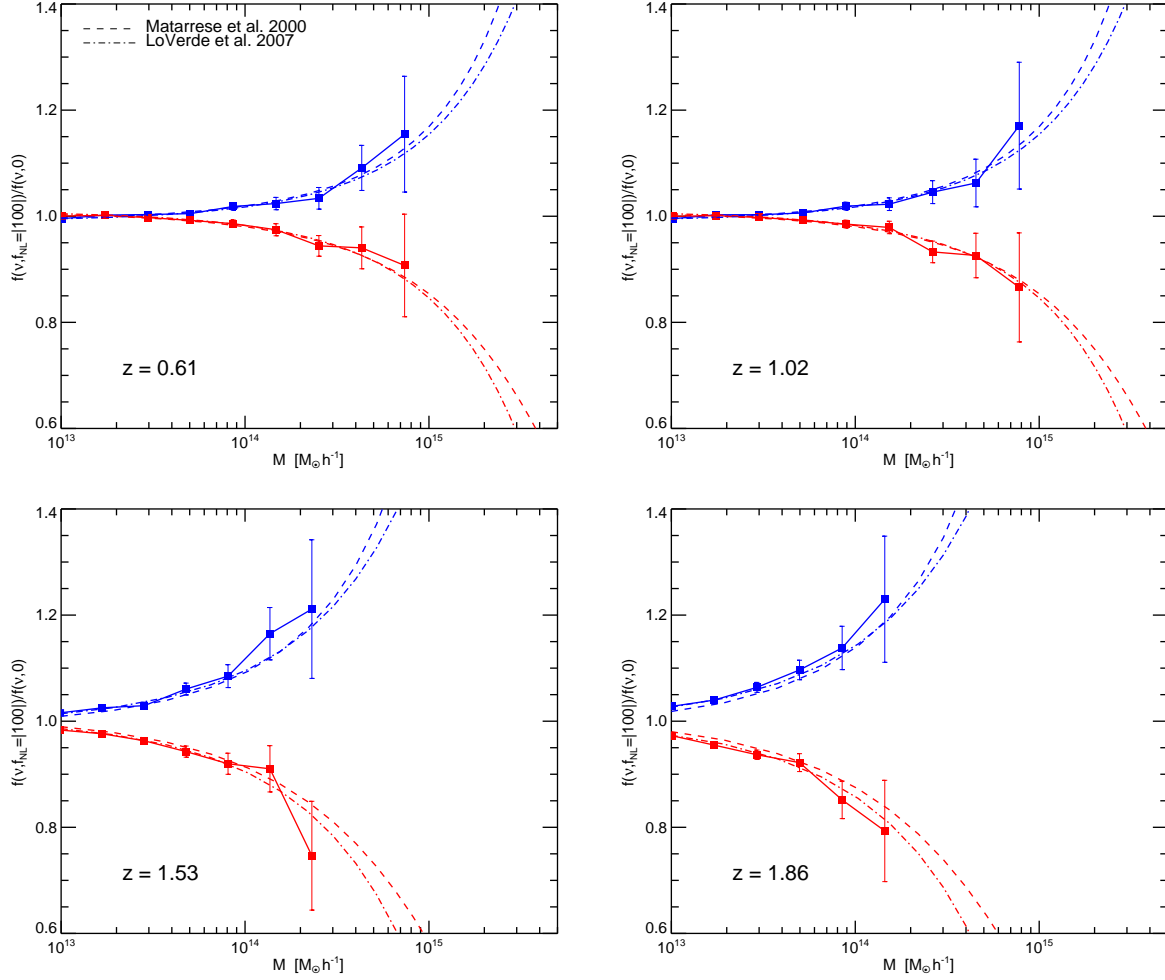


**Figure 6.** Ratio of the non-Gaussian ( $f_{NL} = \pm 100$ ) to Gaussian mass function for different redshift snapshots: top left  $z = 0.61$ ; top right  $z = 1.02$ ; bottom left  $z = 1.53$ ; bottom right  $z = 1.86$ . The dashed line is the mass function of Matarrese, Verde & Jimenez (2001) and the dot-dashed lines are that of LoVerde et al. (2008), both including the  $q$ -correction.

( $M \gtrsim 10^{13} M_{\odot}$ ), it is reliable to assume that the correction from the “non-spherical collapse” can be encapsulated in the factor  $q$  in front of  $\delta_c(z_o)/(\sigma_M^2 D(z_o))$ .

## 6 NON-GAUSSIAN HALO BIAS

Eq. (8) shows that the redshift and scale dependence of the non-Gaussian correction can be factorized as a term that depends only on redshift and one that depends only on  $k$  and  $M$ . The  $M$ -dependence is expected to be very weak at large scales ( $k < 0.03$  h/Mpc). Here we will test the mass, scale and redshift dependence of the non-Gaussian halo bias and we calibrate its normalization on the simulations.

In Fig. 9 we show the dependence on halo mass of  $\Delta b/b_L$ . We define the quantity

$$\mathcal{R}(M) = \left(\frac{\Delta b}{b_L}\right)_s \left(\frac{\Delta b}{b_L}\right)_{theory}^{-1}, \quad (12)$$

where  $(\Delta b/b_L)_{theory}$  is given by Eq. (8). To study the mass dependence, we evaluate the theory at fixed mass  $\bar{M} = 10^{14} M_{\odot}$ . We compute the bias from the simulations

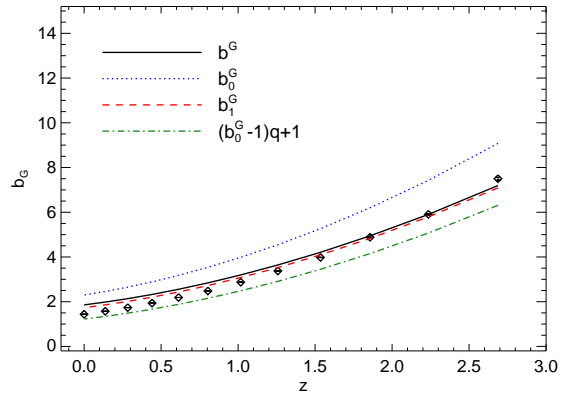


**Figure 8.** Black solid line: the large-scale Gaussian halo Eulerian bias  $b^G$  of Eq. (11). Blue dotted line: the Gaussian halo bias  $b_0^G \equiv 1 + \delta_c(z_o)/(\sigma_M^2 D(z_o))$  as defined in Efsthathiou et al. (1988) and Kaiser (1984). Green dotted-dashed line:  $1 + q(b_0^G - 1)$ . Red dashed line: the contribution  $b_1^G \equiv 1 + [q\delta_c(z_f)/\sigma_M^2 - 1/\delta_c(z_f)]/D(z_o)$  to the total bias of Eq. (11).

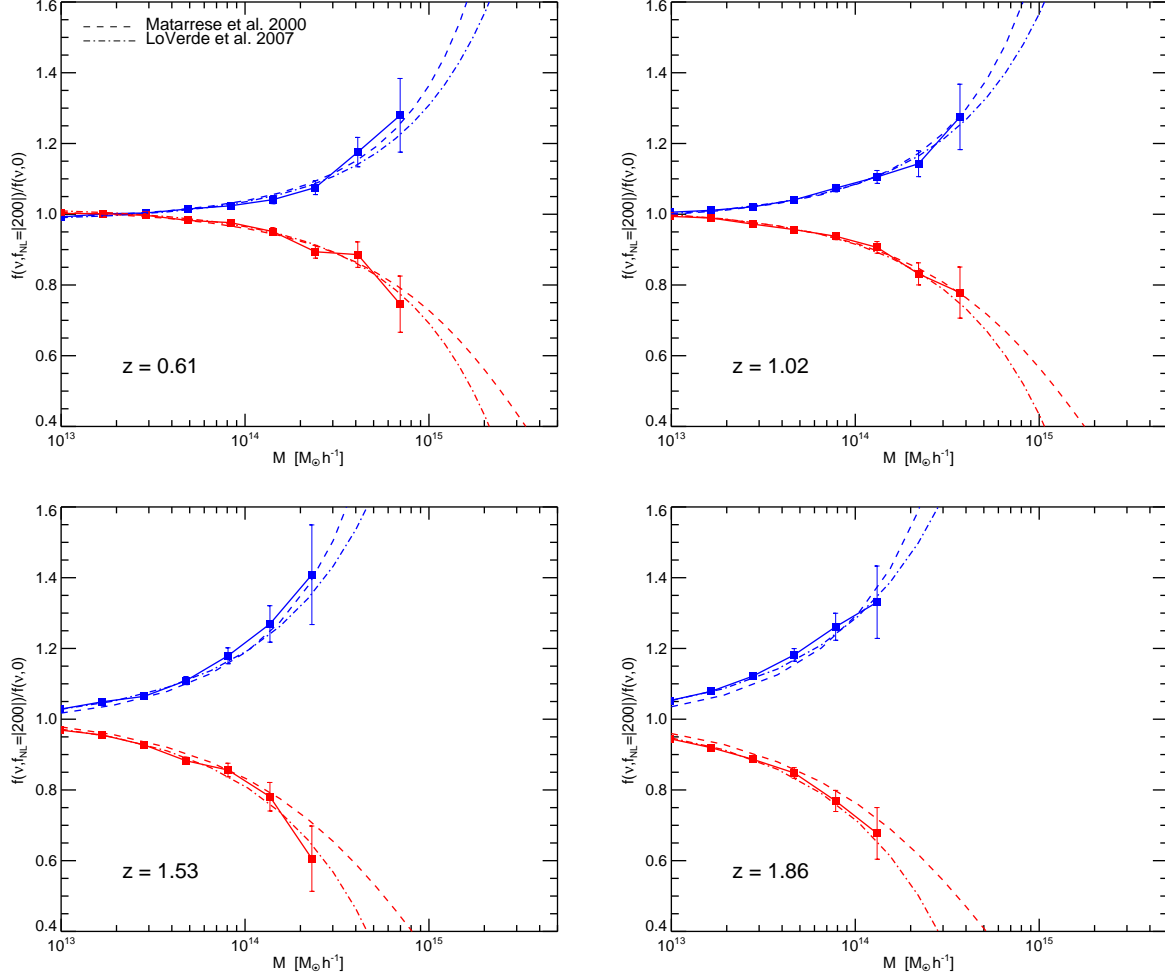


**Figure 7.** Ratio of the non-Gaussian ( $f_{NL} = \pm 200$ ) to Gaussian mass function for different redshift snapshots: top left  $z = 0.61$ ; top right  $z = 1.02$ ; bottom left  $z = 1.53$ ; bottom right  $z = 1.86$ . The dashed line is the mass function of Matarrese, Verde & Jimenez (2001) and the dot-dashed lines are that of LoVerde et al. (2008), both including our  $q$ -correction.

taking halos in six different mass bins. Fig. 9 includes only scales  $k < 0.03 h/\text{Mpc}$ , different lines correspond to different redshift snapshots between  $z = 0$  and  $z = 1.5$ . As expected, there is no noticeable dependence on halo mass.

Having confirmed the expected weak dependence on halo mass for masses  $M > 10^{13} M_{\odot}/h$  and on scales  $k < 0.03 h/\text{Mpc}$ , we can study the redshift and scale dependence of  $\Delta b/b_L$ , considering halos of different masses above  $10^{13} M_{\odot}/h$ .

The redshift dependence of  $\Delta b/b_L$ ,  $(\Delta b/b_L)_s [2f_{NL}\alpha_M(k)q]^{-1}$  is shown in Fig. 10 where  $M > 10^{13} M_{\odot}/h$  and scales  $k < 0.026 h/\text{Mpc}$  were used. In applying the correction  $\delta_c/\sigma_M^2 \rightarrow q\delta_c/\sigma_M^2$  to  $\Delta b/(b_G - 1)$  we have actually corrected  $b_0^G$ , i.e. we have employed the same approximation used for the green dot-dashed line of Fig. 8, giving Eq. (9). Eq.(9) in fact is only the consequence of our correction to the Gaussian halo bias. Note that the approximation  $z_f \sim z_0$  we employed here is expected to hold for rare-massive-halos and Fig. 8 shows that this is a good approximation. A detailed study of the dependence

of the non-Gaussian halo bias correction on the formation redshift of the halos will be presented elsewhere.

There seems to be an indication that the  $q$ -correction factor for the large-scale bias correction may slightly depend on the value of  $f_{NL}$ : in particular the figure shows that it could be slightly smaller than  $q$  for  $f_{NL}$  large and negative and smaller for  $f_{NL}$  large and positive. This is not unexpected: the presence of non-Gaussianity may alter the dynamics of non-spherical collapse (e.g., through tidal forces – see e.g., Desjacques (2008) – or by significantly changing the redshift for collapse with respect to the Gaussian case). At this stage, however, this trend is not highly significant and further study will be left to future work.

Finally, we show the scale dependence of Eq. (9),  $(\Delta b/b_L)_s [2f_{NL}\delta_c(z)q]^{-1}$ , in Fig. 11. The thin lines correspond to different redshifts and the thick black line to their average. The dotted line is the theory prediction with  $q = 0.75$ . Note that there is an excellent agreement on the scales of interest, e.g.,  $k < 0.03 h/\text{Mpc}$ . On smaller scales the effect of non-Gaussianity is very small and the measure-



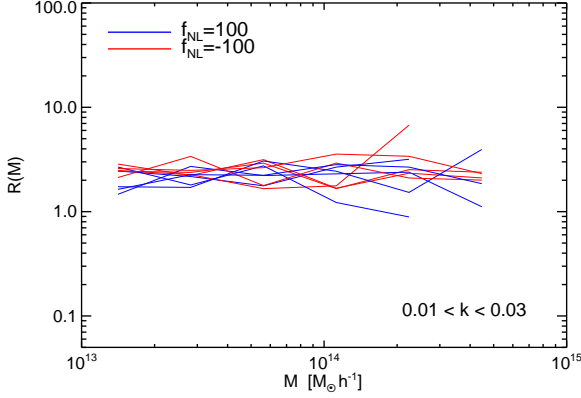


**Figure 9.** Weak mass dependence of  $\Delta b/b$  at scales  $k < 0.03$  h/Mpc. Different lines correspond to different redshift snapshots between  $z = 0$  and  $z = 1.5$ . The overall normalization is arbitrary.

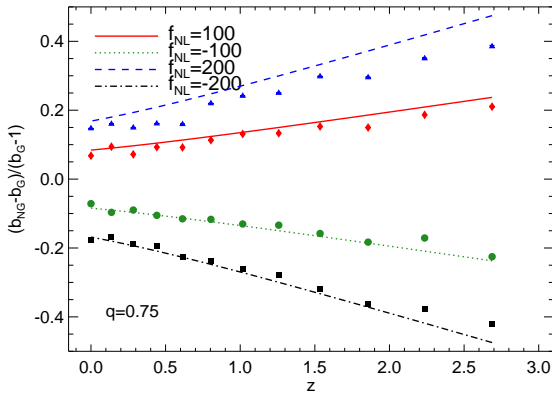


**Figure 10.** The redshift dependence of the non-Gaussian correction to the halo bias: points are the values measured from the simulations, lines are the theoretical predictions, Eq. (9). Only  $k < 0.026$  h/Mpc were used.

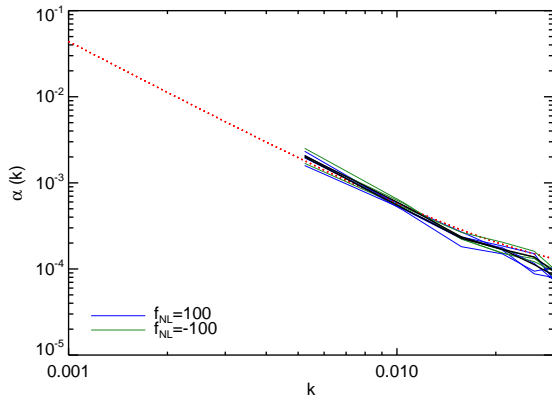


**Figure 11.** Scale dependence of Eq. (9). The thin lines correspond to different redshifts for halos with mass above  $10^{13} M_{\odot}/h$  and the thick black line is their average. The dotted line is the theory prediction with  $q = 0.75$ . At  $k > 0.03$  h/Mpc the effect of non-Gaussianity is very small and the measurement become extremely noisy.

ment become extremely noisy. These results are in qualitative agreement with the findings of Pillepich et al. (2008).

We conclude that Eq. (9), with  $q \sim 0.75$ , provides a good fit to non-Gaussian simulations.

## 7 COMPARISON WITH PREVIOUS WORK

After the discussion of §2, it should be clear that if  $f_{NL}^{CMB}$  were used in the theoretical predictions or  $S_3$  were *not* linearly extrapolated to  $z = 0$ , then any constraints on non-Gaussianity so obtained would have to be re-scaled by a factor  $\sim 1.3$ . This seems to be the case of some work in the literature. On the other hand the  $q$ -correction factor effectively introduces a re-scaling of a factor  $\sim 0.75^{3/2} = 0.65$  for the mass function case and 0.75 for the bias case. It is a coincidence that, for the halo bias,  $1.3 \times 0.75 \sim 1$ , thus the  $f_{NL}$  normalization mistake cancels out with the spherical collapse approximation error. This fortuitous cancellation does not happen to the same level in the mass function  $0.75^{3/2} \times 1.3 \sim 0.8$ , explaining perhaps some of the claimed discrepancy of the simulations with the analytic mass function predictions, and the claimed agreement with the halo bias predictions. Another possible source of inaccuracy would be an inconsistent treatment of the redshift evolution of  $\delta_c$  and  $S_3$  (see discussion in §2).

In Fig. 12 we compare our theoretical predictions with the results presented in Pillepich et al. (2008) and Desjacques et al. (2008). The left panel shows our simulation results at  $z = 0$  for  $f_{NL} = \pm 100$  and our theoretical predictions. Additionally we show the fit presented by Pillepich et al. (2008), Eqs. (8) and (9), evaluated for the suitable values of  $f_{NL}$  accounting for the different notations for  $f_{NL}$ . We also adopt our cosmological parameters when converting  $\sigma_M$  to  $M$ . The right panel shows the simulation results presented in Pillepich et al. (2008) at  $z=0$  and their fitting formula at  $z = 0$  and  $z = 1$ . We over plot our theoretical models evaluated for their cosmological parameters and for the corresponding values of  $f_{NL}$ . Moreover we add the data points from Desjacques et al. (2008) for  $z = 0$  and  $z = 1$ , suitably rescaled by the differences of the  $f_{NL}$  value used. The mass function fits of Fig. 12 differ for large masses, in the regime where simulations errors become large; the fits are however consistent given the individual points error-bars.

Our theoretical formulae for the non-Gaussian mass function (Eqs. 5, 6, 7) and for the non-Gaussian halo bias (Eq. 9) are physically motivated expressions that have been tested on  $N$ -body simulations. They have the advantage over fitting formulae that they can be more robustly interpolated and extrapolated to cosmologies and parameters that have not been directly simulated and they are more robust over parameters ranges where the simulations have low signal-to-noise. Compared to simple fitting formulae, Eq. 6,7 and 9 have the disadvantage that they require the calculation of some numerical integrals. To overcome this, we supply tabulated values for  $S_{3,M}^{(1)}$ ,  $\sigma_M$  and  $\alpha_M$  for a WMAP5 cosmology in the range of interest at [www.ice.csic.es/personal/verde/nongaussian.html](http://www.ice.csic.es/personal/verde/nongaussian.html).

The  $q$ -correction we find here has implications for previously reported and forecasted constraints on non-Gaussianity. In Table 1 we report present and forecasted

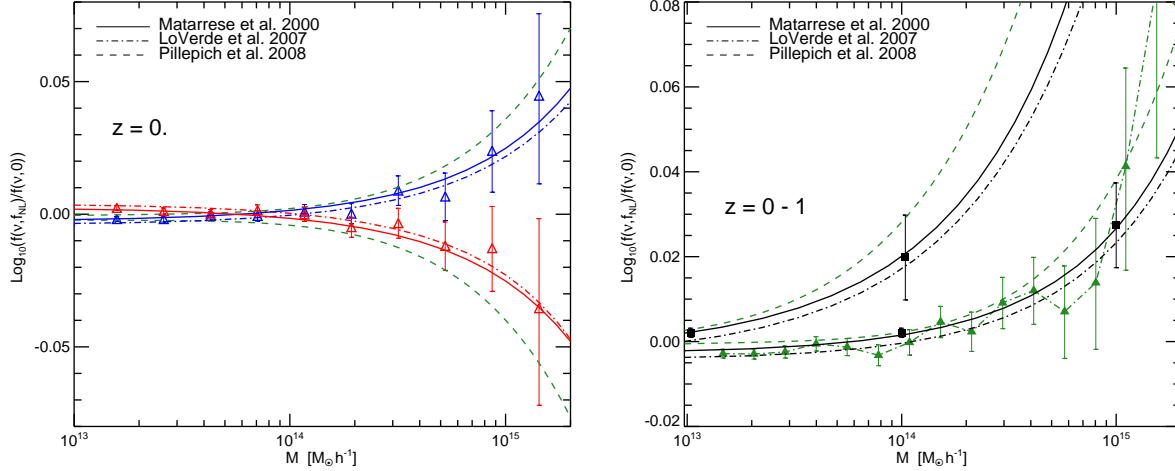


**Figure 12.** Left panel: comparison between simulations points and fits from this work and the polynomial fit of Pillepich et al. (2008). Right panel: Our correction to the Matarrese, Verde & Jimenez (2001) and LoVerde et al (2008) non-Gaussian mass function fits, the polynomial fit of Pillepich, Porciani & Zahn (2009) and points from Desjaques et al (2009) (black squares) and Pillepich, Porciani & Zahn (2009) (green triangles). See text for more details.

constraints on  $f_{NL}$  from the literature rescaled to  $f_{NL}^{CMB}$  and corrected for our factor  $q$ .

This confirms that constraints on  $f_{NL}$  achievable using the non-Gaussian halo bias are competitive with CMB constraints ( $f_{NL} \sim 5$  for Planck and  $f_{NL} \sim 3$  for a CMBPol-type mission, Babich & Zaldarriaga (2004); Yadav, Komatsu & Wandelt (2007)).

## 8 CONCLUSIONS

We have considered  $(1.2 \text{ Gpc}/h)^3$  size and  $960^3$  particles N-body simulations with non-Gaussian initial conditions, with non-Gaussianity parameter  $f_{NL} = \pm 100$ ,  $f_{NL} = \pm 200$  and a reference Gaussian simulation ( $f_{NL} = 0$ ). The clustering properties and the abundance of the simulation's halos were then compared with independent simulations and theoretical predictions. We find good agreement between different simulations, indicating that the initial conditions set-up is under control. We find that the Press-Schechter-based description of the non-Gaussian correction to the Gaussian mass function of Matarrese et al. (2000) and LoVerde et al. (2008) is a good fit to the simulations, provided that:

a) The Press-Schechter-based description is used to compute the ratio between Gaussian and non-Gaussian mass function.

b) The critical density  $\delta_c$  is corrected to account for non-spherical collapse dynamics.

This is summarized in our Eq. (5) and in Eqs. (6) and (7) for the non-Gaussian mass functions of Matarrese et al. (2000) and LoVerde et al. (2008), respectively. For large thresholds this correction is equivalent to a re-scaling of the spherical collapse threshold  $\delta_c \times \sqrt{q}$  where  $q = 0.75$ . The  $q$ -correction is thus equivalent to a reduction of  $f_{NL}$  by a factor  $\sim 1.5$  because in the mass function, to leading order  $f_{NL}$  multiplies  $\delta_c^3$ .

We find that the non-Gaussian halo bias prescription of Dalal et al. (2007), Matarrese & Verde (2008), Slosar et al.

**Table 1.** Current and forecasted constraints on  $f_{NL}^{CMB}$

Data/method	Measurements	reference
	$f_{NL}, 1 - 2\sigma$ errors	
Photo LRG-bias	$84^{+54+85}_{-101-331}$	Slosar et al. 2008
Spectro LRG-bias	$93^{+74+139}_{-83-191}$	Slosar et al. 2008
QSO - bias	$11^{+26+47}_{-37-77}$	Slosar et al. 2008
combined	$37^{+23+42}_{-26-57}$	Slosar et al. 2008
NVSS-ISW	$140^{+647+755}_{-337-1157}$	Slosar et al. 2008
NVSS-ISW	$272 \pm 127$ ( $2-\sigma$ )	Afshordi&Tolley 2008
Data/method	Forecasts	reference
	$\Delta f_{NL}(1 - \sigma)$	
BOSS-bias	18	Carbone et al 2008
ADEPT/Euclid-bias	1.5	Carbone et al. 2008
PANNStarrs-bias	3.5	Carbone et al. 2008
LSST-bias	0.7	Carbone et al. 2008
LSST-ISW	10.	Afshordi&Tolley 2008

(2008) and Afshordi & Tolley (2008) provides a good description of the scaling of the large-scale halo clustering of the simulations. In particular, we have tested separately the predicted redshift, scale and  $f_{NL}$  dependence. The overall

amplitude of the effect, however, should be corrected by a factor  $\sim q$  which can also be understood in the context of ellipsoidal collapse or as a modification to the excursion set ansatz and the sharp-k space filtering (see Eq. (9)). There is an indication that this correction may be slightly dependent on  $f_{\text{NL}}$ . This is not unexpected, but the signal-to-noise of the effect is too small in the current simulations to draw robust conclusions. We also find that on large ( $k < 0.03$   $h/\text{Mpc}$ ) scales, as expected, the fractional correction to the non-Gaussian halo bias is independent of mass. On smaller scales a dependence on mass is expected, but the simulations do not have sufficient signal-to-noise to verify it. The  $q$ -correction to the non-Gaussian halo bias modifies current and forecasted constraints reported in the literature as indicated in our Table 1.

The formulae we presented here for the non-Gaussian mass function (Eq. 5, 6,7) and non-Gaussian halo bias (Eq. 9) are physically motivated expressions which provide good fits to a suite of N-body simulations. As such, they can be more robustly interpolated and extrapolated than simple fitting functions (in [www.ice.csic.es/personal/verde/nongaussian.html](http://www.ice.csic.es/personal/verde/nongaussian.html) we provide useful quantities for ease of use of these equations). We confirm that the non-Gaussian halo bias offers a robust and highly competitive test of primordial non-Gaussianity.

#### ACKNOWLEDGMENTS

Computations have been performed on the IBM-SP5 at CINECA (Consorzio Interuniversitario del Nord-Est per il Calcolo Automatico), Bologna, with CPU time assigned under an INAF-CINECA grant, and on the IBM-SP4 machine at the “Rechenzentrum der Max-Planck-Gesellschaft” at the Max-Planck Institut fuer Plasmaphysik with CPU time assigned to the “Max-Planck-Institut für Astrophysik” and at the “Leibniz-Rechenzentrum” with CPU time assigned to the Project “h0073”. The authors thank A. Pillepich and C. Porciani for discussions and for making available the simulations outputs for comparison. We also thank N. Dalal, U. Seljak, A. Riotto and M. Maggiore for discussions. LV is supported by FP7-PEOPLE-2007-4-3-IRG n. 202182 and CSIC I3 grant n. 200750I034. CC is supported through a Beatriu de Pinos grant. This research was supported by the DFG cluster of excellence Origin and Structure of the Universe. SM and LM acknowledge partial support by ASI contract I/016/07/0 “COFIS”, ASI-INAF I/023/05/0, ASI-INAF I/088/06/0 and ASI contract Planck LFI Activity of Phase E2. LV thanks the Santa Fe cosmology workshop 2008, LV and CC thank the Galileo Galilei Institute for theoretical physics in Florence, where part of this work was carried out, and INFN for partial support. LV thanks B. Wandelt for discussions.

#### REFERENCES

Afshordi, N., & Tolley, A. J. 2008, eprint arXiv:0806.1046  
 Bartolo, N., Komatsu, E., Matarrese, S., & Riotto, A. 2004, Phys.Rep., 402, 103  
 Bartolo, N., Matarrese, S., & Riotto, A. 2005, Journal of Cosmology and Astro-Particle Physics, 10, 10

Babich D., & Zaldarriaga, M. 2004, Phys. Rev. D70, 083005  
 Carbone, C., Verde, L., & Matarrese, S. 2008, ApJL 684, L1  
 Catelan, P., Lucchin, F., Matarrese, S., & Porciani, C. 1998, MNRAS, 297, 692  
 Cole, S., Kaiser, N., 1989, MNRAS, 231, 1127  
 Dalal, N., Dore, O., Huterer, D., & Shirokov, A. 2007, PRD, 77, 123514.  
 Desjacques V., 2008, MNRAS, 388, 638  
 Desjacques, V., Seljak, U., & Iliev, I. T. 2008, arXiv:0811.2748  
 Efstathiou, G., Frenk, C. S., White, S. D. M., Davis, M., 1988, MNRAS, 235, 715  
 Eisenstein, D. J., & Hu, W. 1999, ApJ, 511, 5  
 Gangui, A., Lucchin, F., Matarrese, S., & Mollerach, S. 1994, ApJ, 430, 447  
 Gao, L., Springel, V., & White, S. D. M. 2005, MNRAS, 363, L66  
 Grinstein, B., & Wise, M. B. 1986, ApJ, 310, 19  
 Grossi, M., Dolag, K., Branchini, E., Matarrese, S., & Moscardini, L. 2007, MNRAS, 382, 1261  
 Grossi, M., Branchini, E., Dolag, K., Matarrese, S., & Moscardini, L. 2008, MNRAS, 390, 438  
 Jensen, L. G., & Szalay, A. S. 1986, ApJL, 305, L5  
 Jenkins, A., Frenk, C. S., White, S. D. M., Colberg, J. M., Cole, S., Evrard, A. E., Couchman, H. M. P., & Yoshida, N. 2001, MNRAS, 321, 372  
 Kaiser, N. 1984, ApJL, 284, L9  
 Kang, X., Norberg, P., & Silk, J. 2007, MNRAS, 376, 343  
 Kitayama, T., & Suto, Y. 1996, MNRAS, 280, 638  
 Koyama, K., Soda, J., & Taruya, A. 1999, MNRAS, 310, 1111  
 Komatsu, E., & Spergel, D. N. 2001, PRD, 63, 063002  
 Komatsu, E., et al. 2008, arXiv:0803.0547  
 Lee, J., & Shandarin, S. F. 1998, ApJ, 500, 14  
 LoVerde, M., Miller, A., Shandera, S., & Verde, L. 2008, JCAP 04, 014.  
 Lucchin, F., Matarrese, S., & Vittorio, N. 1988, ApJL, 330, L21  
 Matarrese, S., Lucchin, F., & Bonometto, S. A. 1986, ApJL, 310, L21  
 Matarrese, S., Verde, L., & Jimenez, R. 2000, ApJL, 541, 10  
 Matarrese, S., & Verde, L. 2008, ApJL, 677, L77 (MV08)  
 McDonald, P., eprint arXiv:0806.1061  
 Mo, H. J., Jing, Y. P., White, S. D. M. 1997, MNRAS, 284, 189.  
 Mo, H. J., & White, S. D. M. 1996, MNRAS, 282, 347  
 Pillepich, A., Porciani, C., & Hahn, O. 2008, arXiv:0811.4176  
 Politzer, H. D., & Wise, M. B. 1984, MNRAS, 285, L1  
 Press, W. H., & Schechter, P. 1974, ApJ, 187, 425.  
 Reed, D., Gardner, J., Quinn, T., Stadel, J., Fardal, M., Lake, G., & Governato, F. 2003, MNRAS, 346, 565  
 Robertson, B., Kravtsov, A., Tinker, J., & Zentner, A. 2008, arXiv:0812.3148  
 Robinson, J., & Baker, J. E. 2000, MNRAS, 311, 781  
 Robinson, J., Gawiser, E., & Silk, J. 2000, ApJ, 532, 1  
 Salopek, D. S., & Bond, J. R. 1990, PRD, 42, 3936  
 Scoccamarro, R., Sheth, R., Hui, L. & Jain, B. 2001, ApJ, 546, 20.  
 Seljak, U., eprint arXiv:0807.1770.

- Sheth, R. K., Mo, H. J., & Tormen, G. 2001, MNRAS, 323, 1
- Sheth, R. K. 1998, MNRAS, 300, 1057
- Sheth, R. K., & Tormen, G. 1999, MNRAS, 308, 119
- Sheth, R. K., & Tormen, G. 2002, MNRAS, 329, 61
- Slosar, A., Hirata, C., Seljak, U., Ho, S., & Padmanabhan, N. 2008, 2008, JCAP, 08, 031.
- Springel, V. 2005, MNRAS, 364, 1105
- Verde, L., Jimenez, R., Kamionkowski, M., & Matarrese, S. 2001, MNRAS, 325, 412
- Verde, L., Wang, L., Heavens, A. F., & Kamionkowski, M. 2000, MNRAS, 313, 141
- Viel, M., Branchini, E., Dolag, K., Grossi, M., Matarrese, S., & Moscardini, L. 2009, MNRAS, 393, 774
- Warren, M. S., Abazajian, K., Holz, D. E., & Teodoro, L. 2006, ApJ, 646, 881
- Yadav, A.P.S., Komatsu, E. & Wandelt, B.D. 2007, ApJ, 664, 680